PHYSICAL REVIEW E **71**, 065601(R) (2005)

Self-channeling of ultrashort laser pulses in materials with anomalous dispersion

L. Bergé[1] and S. Skupin[1,2]
[1]*Département de Physique Théorique et Appliquée, CEA/DAM Ile de France, B.P. 12, 91680 Bruyères-le-Châtel, France*
[2]*Institute of Condensed Matter Theory and Solid State Optics, Friedrich-Schiller-Universität Jena, Max-Wien-Platz 1, 07743 Jena, Germany*

(Received 17 February 2005; published 16 June 2005)

The nonlinear dynamics of femtosecond optical pulses propagating in solid media with anomalous group-velocity dispersion (GVD) is investigated. A map fixing the boundaries of collapse or noncollapse regimes for high-power beams versus the relative strength of GVD is first established. Next, from a nonlinear Schrödinger model accounting for higher-order dispersion, self-steepening, and plasma generation, the possibility of producing extended collapse events that promote a long self-guiding is confirmed, in agreement with recent experiments [K.D. Moll and A.L. Gaeta, Opt. Lett. **29**, 995 (2004)]. Three-dimensional collapsing pulses are shown to propagate by emitting quasiperiodically bursts of temporally compressed light bullets, with durations close to the single cycle limit.

DOI: 10.1103/PhysRevE.71.065601 PACS number(s): 42.65.Tg, 42.65.Jx, 42.25.Bs

With the development of ultrashort laser sources, the propagation of femtosecond pulses in transparent media have led to a large variety of unique phenomena, including the appearance of self-guided filaments over long distances in air [1], pulse shortening, and supercontinuum generation [2–5]. These processes usually originate from the early self-focusing of the beam, which causes an important growth of the laser intensity. Depending on the respective weights of dispersion versus the input peak power, the beam collapse can be halted by either chromatic dispersion [3] or by plasma generation [4]. The resulting filament can then continue to propagate inside the medium in the form of a narrow light channel.

Whereas attention was mostly paid on femtosecond pulses undergoing normal group-velocity dispersion (GVD), fewer studies were devoted to the influence of anomalous GVD. From the mathematical point of view, the possibility of creating "light bullets" in $(2+1)$-dimensional media, stabilized by higher-order dispersion without plasma generation, was reported in [6]. For a cubic nonlinearity, fourth-order dispersion is indeed able to regularize the wave blowup for one-dimensional (1D) spatial diffraction and anomalous GVD. This property, however, does not hold in $(3+1)$ dimensions, for which collapse still occurs [6]. From the experimental point of view, only one paper recently dealt with this fascinating dynamics [7]. Here, 50-fs pulses were focused into a BK7 glass sample at different laser wavelengths leading to normal or anomalous GVD. With normal GVD, the pulse developed short, multiple self-focusing events, guiding the beam within one Rayleigh length only. In contrast, with anomalous GVD, collapse events appeared over many Rayleigh lengths, giving rise to a long "segment" of light followed by shorter focusing-defocusing cycles at high enough powers. In [7], numerical problems prevented the authors from examining the collapse dynamics for long interaction lengths. A detailed picture of the pulse evolution subject to anomalous GVD is thus missing, which justifies the purpose of the present work.

Here, we theoretically investigate the dynamics of ultrashort pulses undergoing anomalous GVD in fused silica. First, for Gaussian pulses, we elaborate on a map delimiting the zones of collapse (self-focusing) as a function of the normalized dispersive coefficients versus the ratio of peak input power over critical. Second, numerical simulations display evidence of the extended-collapse regime discovered in [7]. Third, we detail the pulse dynamics. This relies on a strong temporal compression that triggers an electron plasma and confines the pulse to its back part. This particular behavior produces wave packets compressed to the few-cycle limit.

The electric-field envelope $\mathcal{E}(r,t,z)$ is governed by a nonlinear Schrödinger (NLS) equation expressed in the frame moving with the group velocity $v_g=1/k^{(1)}$ $(t\to t-k^{(1)}z)$ and coupled with a Drude model that describes the growth of the free-electron density $\rho(r,t,z)$, as

$$\frac{\partial}{\partial z}\mathcal{E}=\frac{i}{2k^{(0)}}T^{-1}\nabla_\perp^2\mathcal{E}+i\hat{D}\mathcal{E}-i\frac{k^{(0)}}{2n_0^2\rho_c}T^{-1}\rho\mathcal{E}-\frac{\sigma}{2}\rho\mathcal{E}+i\frac{\omega_0}{c}n_2T|\mathcal{E}|^2\mathcal{E}-\frac{\beta^{(K)}}{2}|\mathcal{E}|^{2K-2}\mathcal{E}, \tag{1a}$$

$$\frac{\partial}{\partial t}\rho=\sigma_K\rho_{\rm nt}|\mathcal{E}|^{2K}+\frac{\sigma}{U_i}\rho|\mathcal{E}|^2-\frac{1}{\tau_r}\rho. \tag{1b}$$

In Eq. (1a), z denotes the propagation variable, $k^{(0)}=n_0\omega_0/c$ is the central wave number in silica ($n_0=1.45$), the operator $\nabla_\perp^2=r^{-1}\partial_r r\partial_r$ accounts for diffraction, and $\hat{D}=\Sigma_{n=2}^{5}(k^{(n)}/n!)(i\partial_t)^n$ is the dispersion operator. The dispersion coefficients $k^{(n)}\equiv\partial^n k/\partial\omega^n|_{\omega=\omega_0}$ are computed from a Sellmeier formula for bulk fused silica given in Ref. [8] (higher orders $n>5$ were checked to have no influence on the pulse dynamics). The following terms of Eq. (1a) describe plasma coupling with ρ_c being the critical plasma density and σ the cross section for inverse bremsstrahlung. The next one refers to the Kerr response of the medium with nonlinear coefficient n_2 while the last contribution accounts for K-photon absorption with $\beta^{(K)}=K\hbar\omega_0\rho_{\rm nt}\sigma_K$. Equation (1a) includes

space-time focusing ($T^{-1}\nabla_\perp^2\mathcal{E}$) and self-steepening ($T|\mathcal{E}|^2\mathcal{E}$), where $T\equiv 1+(i/\omega_0)\partial_t$ [4,10]. Equation (1b) describes plasma generation, namely, multiphoton ionization (MPI) with rate σ_K [9] and initial neutral density $\rho_{\rm nt}=2.1\times10^{22}$ cm^{-3}, avalanche ionization for the gap potential $U_i=7.8$ eV, and electron recombination with characteristic time $\tau_r=150$ fs [5]. In anomalous GVD regimes, the laser wavelength is fixed to $\lambda_0=1550$ nm, for which $k''=-280$ fs^2/cm, $k'''=1500$ fs^3/cm, $k''''=-4900$ fs^4/cm, $k^{(v)}=23\,000$ fs^5/cm, $n_2=2.2\times10^{-16}$ cm^2/W, $\rho_c=4.6\times10^{20}$ cm^{-3}, $\sigma=2.1\times10^{-18}$ cm^2, $\sigma_K=1.9\times10^{-120}$ s^{-1} cm^{2K}/W^K, and the number of photons required for ionization is $K=10$. For further comparisons with normal GVD regimes, we shall consider the wavelength $\lambda_0=790$ nm with the ionization parameters of Ref. [4], leading in particular to $k''=370$ fs^2/cm, $k'''=270$ fs^3/cm and $K=5$. Gaussian pulses launched in parallel geometry, $\mathcal{E}_0=\sqrt{2P_{\rm in}/\pi w_0^2}e^{-r^2/w_0^2-t^2/t_p^2}$, with input waist w_0, power $P_{\rm in}$ and half-width duration t_p [=full width at half maximum(FWHM)/$\sqrt{2\ln 2}$] will serve as initial conditions for Eqs. (1). The critical power for self-focusing takes the value $P_{\rm cr}=\lambda_0^2/2\pi n_0 n_2\simeq 12$ MW at $\lambda_0=1550$ nm.

We first investigate under which condition collapse with anomalous GVD may occur or not. Here, "collapse" means extensive plasma generation triggered by self-focusing. Since higher-order dispersion cannot arrest the wave blowup in (3+1) dimensions [6], we can consider the academic three-dimensional (3D) NLS equation to be a good approximation of the full system (1) in the self-focusing regime. This well-known equation reads

$$i\frac{\partial}{\partial z}\psi+\nabla_\perp^2\psi+\frac{\partial^2}{\partial t^2}\psi+|\psi|^2\psi=0, \qquad (2)$$

and follows from Eq. (1a) in the limits $T=1$, $\rho\to 0$, after simple rescalings [4] that involve the Rayleigh length $z_0=n_0\pi w_0^2/\lambda_0$ and the dispersion length $L_D=t_p^2/|k''|$. The rescaled input $\psi_0=\sqrt{8p}\exp(-r^2-\delta_2 t^2)$ shows that the occurrence of collapse is determined by the normalized GVD coefficient $\delta_2=2z_0/L_D$ and the power ratio $p\equiv P_{\rm in}/P_{\rm cr}$ only. Following Ref. [11], for given initial mass $N=\int|\psi_0|^2d\vec{r}dt=(2\pi)^{3/2}p/\sqrt{\delta_2}$, gradient norm $X_0=\int(|\nabla_\perp\psi_0|^2+|\partial_t\psi_0|^2)d\vec{r}dt=N(2+\delta_2)$, and Hamiltonian $H=X_0-\frac{1}{2}\int|\psi_0|^4d\vec{r}dt=X_0-N\sqrt{2}p$, three characteristic regions exist: For $X_0>\widetilde{X}\equiv 3N_s^2/N$, $H<\widetilde{H}\equiv N_s^2/N$, where $N_s=18.94$ denotes the mass of the ground-state soliton for Eq. (2) [11], collapse is unavoidable. For $X_0<\widetilde{X}$, $H<\widetilde{H}$, collapse is forbidden. Collapse is optional in the remaining regions. Figure 1 shows these three regions in the plane (δ_2,p), delimited by solid lines. To verify our reasoning, we performed numerical integrations of the *complete* system (1) with different values of p and $|\delta_2|$. Open circles represent the initial conditions that do not collapse, i.e., they spread out after a possible stage of smooth intensity growth. In contrast, closed circles mark the input conditions that do collapse, i.e., the wave intensity increases by more than one decade before producing a peak electron density $\rho_{\rm max}>10^{18}$ cm^{-3}. We observe that the blowup regions inferred from the 3D NLS equation are still valid for the full model equations. Moreover, the dashed line ($\widetilde{X}=X_0$) approximately divides the plane in collapsing and noncollapsing regimes, and may be used as a first clue to evaluate their boundary. Several data were thoroughly tested by discarding either third- and/or fourth-order dispersion, or by setting T,T^{-1} equal to unity. None of these modifications, however, altered the collapse points shown in Fig. 2, within a power increment of $\Delta p=0.5$. The general trend, that the power threshold for collapse increases with δ_2, can be understood as follows. For $\delta_2\to 0$, the diffraction length $2z_0$ is much shorter than the dispersion length L_D and we observe genuine (2+1)-dimensional collapse for $p\gtrsim 1$ in the (x,y) plane. Reversely, for $\delta_2\to\infty$, diffraction becomes negligible and the pulse tends to evolve with (1+1)-dimensional noncollapsing dynamics.

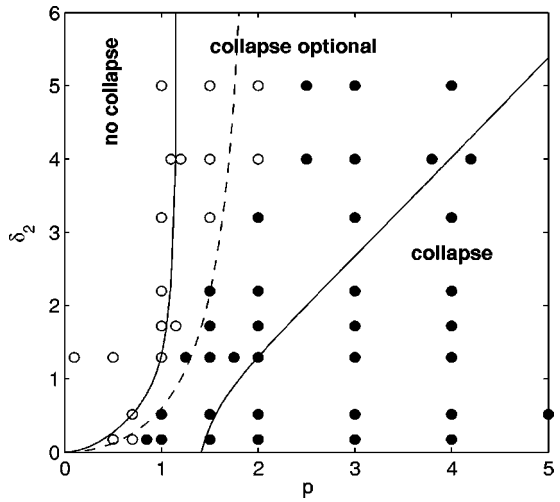

FIG. 1. Collapse regions plotted as $\delta_2\equiv 2z_0/L_D$ vs $p\equiv P_{\rm in}/P_{\rm cr}$. The dashed line represents the frontier between the ground-state and input gradient norms for Eq. (2), $\widetilde{X}=X_0$.

From now on, we analyze the self-guiding properties of collapsing pulses at 1550 nm. Figures 2(a)–2(d) show the maximum optical intensity (units are indicated on the left-hand-side axis) and peak electron density (resp. right-hand-side axis) for different pulse powers. Input beam waist is $w_0=71$ μm ($z_0=1.5$ cm) and $t_p=42.5$ fs ($\delta_2=0.46$). Starting from $p=1$ yields a single collapse sequence [Fig. 2(a)]. At increasing powers, the pulse undergoes more and more focusing-defocusing events while the first collapse point becomes closer to $z=0$. Collapse cycles are repeated [Fig. 2(b)] until the pulse develops a large "block" or "segment" of high-intensity light, i.e., the self-guiding occurs within an extended zone clamped with a quasiconstant plateau of free electrons [Fig. 2(c)]. The typical waist of the filament is 10–20 μm. By augmenting $P_{\rm in}$ again, this block decays into bursts of collapsing structures that prolong the self-channeling over more than three Rayleigh lengths [Fig. 2(d)]. The primary extended zone of collapse occupies the first cm range along the optical path; the secondary bursts take place over $\sim$0.5 cm each. This dynamics is in excellent agreement with the experimental data reported in Ref. [7]. For comparison, Fig. 2(e) shows an example of self-guiding at $\lambda_0=790$ nm, i.e., for normal GVD, using the same waist and pulse duration. In that case, focusing-defocusing events

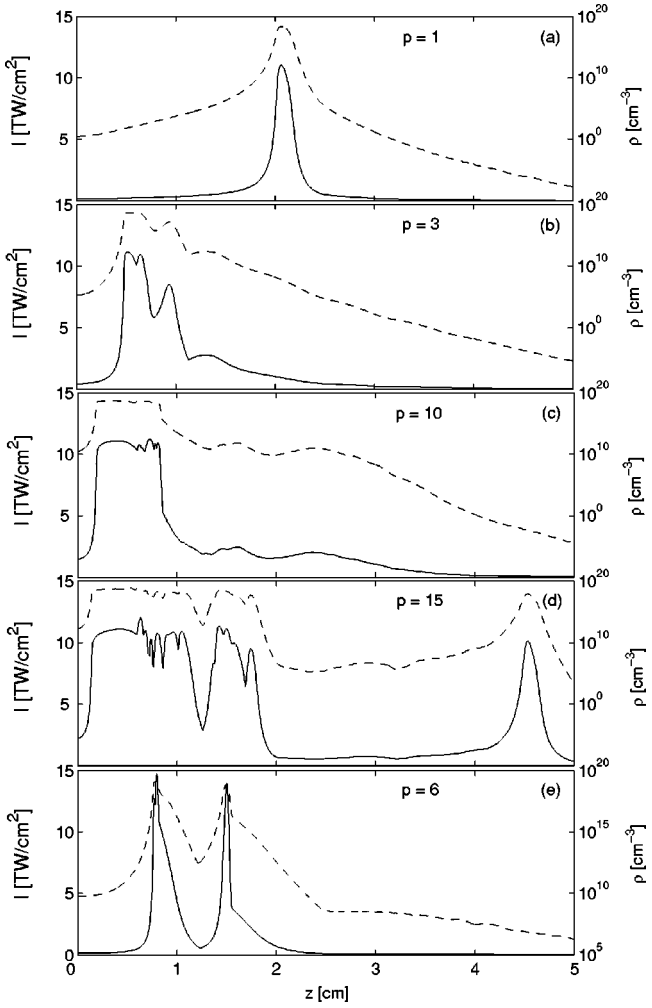

FIG. 2. Peak intensities (solid curves) and electron densities (dashed curves) for 1550-nm pulses at various powers (w_0 =71 μm, t_p=42.5 fs). The last frame (e) shows the same quantities at 790 nm.

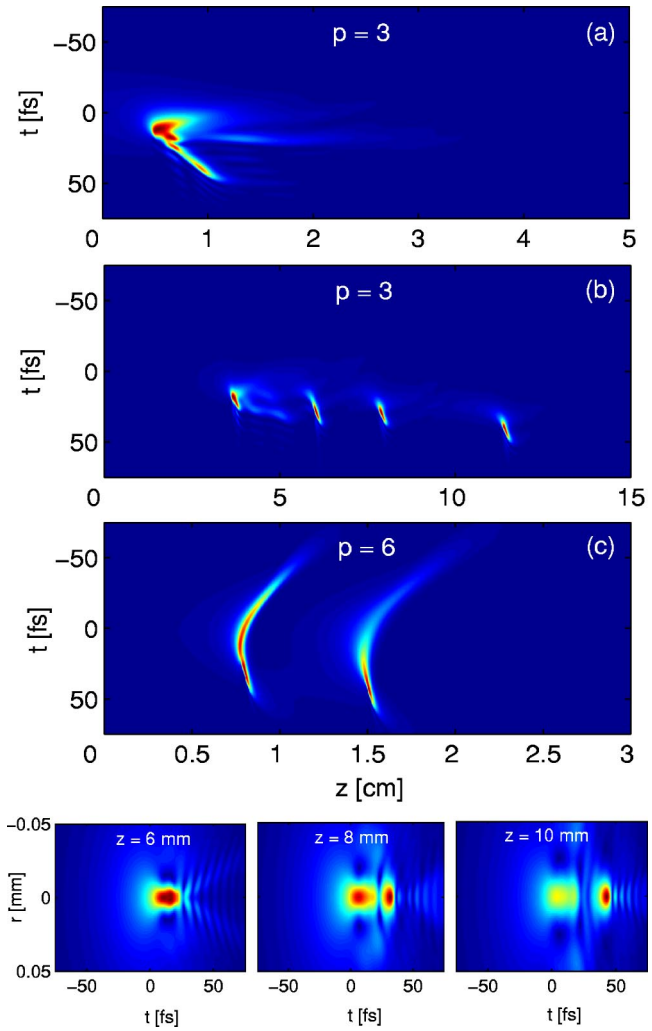

FIG. 3. Temporal dynamics of (a) 42.5-fs pulse at 1550 nm with p=3 and w_0=71 μm, (b) 75-fs pulse at 1550 nm with p=3 and w_0=200 μm, (c) 42.5-fs pulse at 790 nm with p=6 and w_0 =71 μm. Bottom inset: Single focusing-defocusing sequence in the plane (r,t) for the configuration (a).

arise in the form of very localized spikes staying below the Rayleigh distance $z_0 \simeq 3$ cm, which again agrees with [7].

Figure 3(a) displays the temporal evolution along the propagation axis for the pulse used in Fig. 2(b). The temporal profile starting from a FWHM of 50 fs shrinks, due to the collapse dynamics that forces a compression in all space and time directions. The pulse is then confined into a thin structure pushed to positive times. More precisely, the first plasma stage defocuses the back of the pulse, and earlier time slices can refocus at larger z distances. As these slices increase, they still compress temporally and undergo both third-order dispersion and self-steepening, which make them shift to more positive instants. As a result, the pulse can propagate over long distances by emitting very short optical structures. This phenomenon is generic and can even be amplified with a larger waist [w_0=200 μm, Fig. 3(b)]. Here, the first collapse region is followed by a quasiperiodic emission of bursts of wave packets shortened in time and pushed to the very back of the pulse. Figure 3(c) shows the propagation dynamics at 790 nm. Normal GVD is responsible for stretching the pulse along time. Although the trail is again amplified by self-steepening, defocused components are rapidly pushed back to negative times. The bottom inset of Fig. 3 details the temporal distortions of a pulse with 71 μm waist and λ_0 =1550 nm (p=3). At z=6 mm, the pulse self-focuses towards positive times and develops a shock dynamics due to self-steepening. On its trailing edge, plasma defocusing comes into play and permits evacuation of the energy to earlier times (z=8 mm). The pulse is then pushed again to the extreme rear region (z=1 cm), where it confines into a highly focused state. The same dynamics drives the emergence of the small cells emitted at longer distances with a larger waist [Fig. 3(b)]. It also supports the primary long segment of light [Fig. 2(c)], maintained by powerful time slices located near t=0. These central slices keep their intensity close to the ionization threshold over $\sim z_0$, while later components ($t>0$) sharply move to the back of the pulse.

Because anomalous GVD favors time compression, it may be used to produce light pulses with shortened durations. Figure 4(a) shows on-axis temporal profiles produced

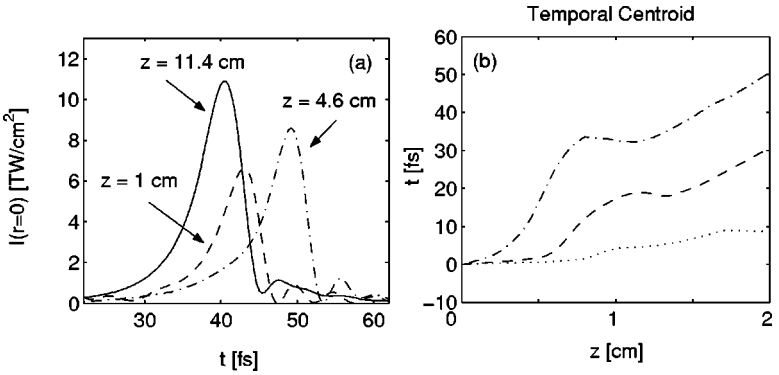

FIG. 4. (a) Temporally compressed 1550-nm pulses at the distances of maximal shortening in time. (b) Temporal centroid motion for anomalous and normal GVD. For $\lambda_0=1550$ nm, pulses have the following parameters: $w_0=200$ μm, $t_p=75$ fs, $p=3$ (solid line), $w_0=71$ μm, $t_p=42.5$ fs, $p=3$ (dashed line), same with $p=15$ (dash-dotted line). For $\lambda_0=790$ nm, $w_0=71$ μm, $t_p=42.5$ fs, and $p=6$ are used (dotted line).

by the Gaussian pulses examined in Figs. 2 and 3. The indicated distances correspond to the locations upon the z axis, where a minimal duration is reached. Self-focusing and defocusing events provide optical wave packets with a FWHM duration shrunk to 5–10 fs, i.e., lying in the limit of two optical cycles ($\tau_{oc}=\lambda_0/c=5$ fs) for which Eqs. (1) remain valid [10]. Such ultraconfined pulses experience strong backward motions. Figure 4(b) illustrates the temporal centroid of the entire pulse $\langle t\rangle \equiv \int t|\mathcal{E}|^2 d\vec{r}dt / \int |\mathcal{E}|^2 d\vec{r}dt$. Computed from the previous examples, this centroid is pushed to the latest time slices of the pulse. This property can be understood from the evolution of the integral $\mathcal{M}_t \equiv \int t|\mathcal{E}|^2 d\vec{r}dt$,

$$\frac{d}{dz}\mathcal{M}_t = \frac{1}{2k^{(0)}\omega_0}\int |\nabla_\perp \mathcal{E}|^2 d\vec{r}dt + \frac{3n_2}{2c}\int |\mathcal{E}|^4 d\vec{r}dt + \frac{k'''}{2}\int \left|\frac{\partial}{\partial t}\mathcal{E}\right|^2 d\vec{r}dt - k''\int |\mathcal{E}|^2 \frac{\partial}{\partial t}\arg\{\mathcal{E}\} d\vec{r}dt, \tag{3}$$

where fourth- and fifth-order dispersions have been discarded because of their weak influence on the pulse dynamics, which was numerically verified through various pulse configurations.

Equation (3) shows that space-time focusing, self-steepening [first and second terms in the right-hand side of Eq. (3)], and third-order dispersion participate in pushing the temporal centroid of the pulse to positive instants. The GVD contribution [last integral in Eq. (3)] was checked to be negligible in all simulations performed. Third-order dispersion, being five times higher at 1550 nm than at 790 nm, amplifies the centroid motion to the back of the pulse for the former wavelength.

In summary, we have shown that anomalous GVD maintains the self-channeling of ultrashort pulses by continuously reinjecting energy into the self-focusing region, owing to the temporal compression that characterizes a 3D collapse. This dynamics, proposed in Ref. [7], has been confirmed by several numerical simulations, which reproduced the experimental features, i.e., the occurrence of a primary long segment of light followed by bursts of optical collapse events. We analytically determined the zones in the plane $(2z_0/L_D, P_{in}/P_{cr})$, where the collapse is strictly forbidden and where it triggers plasma generation. Next, we identified the temporal dynamics sustaining the self-guiding mechanism with anomalous GVD. We showed that the beam is clamped upon long distances at its peak saturation intensity, because the pulse temporal components are always compressed and shifted to the back of the pulse through self-steepening and third-order dispersion. This evolution favors the quasiperiodic formation of narrow, self-compressed cells of light, whose typical duration can reach the optical cycle limit. This property could open new trends to produce few-cycle laser pulses. We recall for this purpose that plasma generation does not constitute a drawback in pulse-shortening techniques [12], which could even be optimized by operating in anomalously dispersive regimes. Numerical simulations were performed on the HP alpha cluster (CCRT) of CEA-France and on the IBM p690 cluster (JUMP) of the Forschungs-Zentrum in Jülich-Germany.

[1] A. Braun *et al.*, Opt. Lett. **20**, 73 (1995); See, for review, J. Kasparian *et al.*, Science **301**, 61 (2003).
[2] A. L. Gaeta, Phys. Rev. Lett. **84**, 3582 (2000).
[3] M. Kolesik, G. Katona, J. V. Moloney, and E. M. Wright, Phys. Rev. Lett. **91**, 043905 (2003); M. Kolesik, E. M. Wright, and J. V. Moloney, *ibid.* **92**, 253901 (2004).
[4] H. Ward and L. Bergé, Phys. Rev. Lett. **90**, 053901 (2003); S. Champeaux and L. Bergé, Phys. Rev. E **68**, 066603 (2003).
[5] S. Tzortzakis *et al.*, Phys. Rev. Lett. **87**, 213902 (2001).
[6] G. Fibich and B. Ilan, Opt. Lett. **29**, 887 (2004).
[7] K. D. Moll and A. L. Gaeta, Opt. Lett. **29**, 995 (2004).
[8] G. P. Agrawal, *Fiber-Optic Communication Systems*, 2nd ed., (Wiley-Interscience, New York, 1997).
[9] L. V. Keldysh, Sov. Phys. JETP **20**, 1307 (1965).
[10] T. Brabec and F. Krausz, Phys. Rev. Lett. **78**, 3282 (1997).
[11] E. A. Kuznetsov, J. Juul Rasmussen, K. Rypdal, and S. K. Turitsyn, Physica D **87**, 273 (1995).
[12] N. L. Wagner *et al.*, Phys. Rev. Lett. **93**, 173902 (2004).